The effect of circuit parameters on ferroresonant solutions in an LCR circuit

1998 J. Phys. A: Math. Gen. 31 7065

(http://iopscience.iop.org/0305-4470/31/34/010)

J. Phys. A: Math. Gen. **31** (1998) 7065–7076. Printed in the UK PII: S0305-4470(98)89529-2

The effect of circuit parameters on ferroresonant solutions in an LCR circuit

H Lamba†, S McKee‡ and R Simpson§

† SCCM Program, Division of Mechanics and Computation, Stanford University, CA 94305-4040, USA

‡ Department of Mathematics, University of Strathclyde, Glasgow G1 1XV, UK

§ Department of Electronic and Electrical Engineering, University of Strathclyde, Glasgow G1 1XW, UK

Received 26 November 1997, in final form 19 June 1998

Abstract. We use the Preisach model to easily and accurately match the magnetic response of a laboratory-scale transformer and numerically simulate a series LCR circuit. Excellent agreement is obtained with experiment over a wide range of parameters for both non-resonant and ferroresonant behaviour. We then use each of the system's three independent parameters as bifurcation parameters and search for additional ferroresonant solutions, thus demonstrating the potential predictive power of such simulations.

1. Introduction

The study of magnetic circuits is of great importance in electrical engineering. The use of transformers and inductors is universal in power generation and distribution networks.

The magnetic response of a transformer is approximately linear for low values of the applied magnetic field (i.e. low currents and voltages) and thus the linear theory can accurately determine the normal operating state of the system. However, all magnetic characteristics must saturate at large applied fields and at intermediate field strengths the phenomenon of magnetic hysteresis also becomes significant. Thus, there may exist other stable states at the same parameter values as the normal operating state which have higher currents and voltages. These co-existing solutions have been termed *ferroresonant* when they have been observed by engineers.

If the magnetic characteristic is assumed to be linear then the solution of the basic equation is referred to as the non-resonant response. If the magnetic characteristic is nonlinear then at least two stable states can occur. If the result has a significant one-third harmonic of the main frequency then the circuit is said to be operating in a subharmonic state. When the current peak amplitude is very large, 20–30 times the normal, then the circuit is said to be exhibiting main resonance. These have been observed and have been well known to engineers for many years (see e.g. [1]).

Many models have been used to represent the B–H characteristic and these can be broadly classified into two groups. In the first group, the flux density is described by a single-valued function of the applied magnetic field, e.g. by linear, piecewise-linear, polynomial or trigonometric functions. Using such functions it is possible to apply analytic methods such as harmonic balance to obtain results on the amplitudes and regions of stability of certain types of ferroresonant solution [2–7]. However, single-valued functions cannot represent

0305-4470/98/347065+12$19.50

effects due to magnetic hysteresis. Previous work [8, 9] and the authors' experience with laboratory-scale transformers have shown that these effects are significant in two different ways. First some ferroresonant solutions may not exist in the numerical simulation. Second, the residual magnetization of the transformer at start-up can determine whether the non-resonant (normal operating) solution or a ferroresonant solution is achieved. For these reasons we believe that the use of such single-valued representations is not sufficient for accurate modelling of magnetic circuits.

The second group of models, which are much closer to the observed behaviour of real materials, do include magnetic hysteresis effects and the B–H loops are no longer representable by single-valued functions. Examples are the Preisach [10] and Jiles–Atherton models [11]. These models suffer from two drawbacks. First it is much harder to accurately fit an experimentally determined magnetic characteristic and second the resulting circuit equations are likely to be analytically intractable. We shall show how to match the Preisach model to a given B–H characteristic and obtain excellent agreement over a wide range of operating conditions for a sinusoidally driven series LCR circuit. This is one of the simplest circuits capable of ferroresonant behaviour and has been studied previously [4, 5, 7, 12, 13] as a model for a single-phase transformer; yet even this simple circuit is still poorly understood.

The paper is organized as follows. In section 2 we show how to fit the Preisach model, based upon the results in [14, 15], to a given transformer characteristic using solely the measurements of the upper bounding curve of the major hysteresis loop. In section 3 we incorporate the Preisach model into the equation for a series LCR circuit and describe how to numerically integrate the system. Then we compare the numerical simulation with experimental results for an actual laboratory transformer at a particular set of parameter values where there exists a non-resonant solution and two ferroresonant solutions. We show that all three solutions are accurately simulated by comparing the current waveforms. Then in section 4 we perform a computer search for additional ferroresonant solutions by varying each independent parameter in turn and randomly choosing initial conditions and remanence conditions.

2. The Preisach model

The Preisach model [10] is still one of the best mathematical descriptions of magnetic hysteresis available and is potentially extremely accurate. A detailed description of the model and its numerical implementation can be found in [16]. A major problem with applying the Preisach theory is that it requires the accurate determination of a two-parameter function $F(\alpha, \beta)$ (see [8]) (obeying certain mathematical constraints) which represents the magnetic response. This perhaps explains why the Preisach theory has been used so little in numerical simulations.

For a more detailed description of the Preisach theory the reader is referred to [8] (or [16]); it will be assumed that the reader is cognizant with [8] and we shall employ the notation of that paper. Our procedure for determining the two-parameter function F is, however, a little different from [8] and so this section will deal with how this function was approximated.

An elegant approach to approximating F is given in [15] which only requires the upper bounding B–H curve, say, to be measured. This can be done by taking the inductor core close to positive saturation and then reducing the applied field, taking measurements until the core is close to negative saturation.

Let the upper bounding curve of the hysteresis loop be $f^+(H)$ and the lower curve be $f^-(H)$. By symmetry, we must have that $f^-(H) = -f^+(-H)$ so let us assume that the

upper curve has been measured experimentally and fitted by a smooth approximating curve, which we henceforth refer to as $f^+(H)$.

Then

$$F(\alpha, \beta) = \frac{-f^+(\beta) - f^-(\alpha)}{2} + \int_{-\infty}^{\beta}\int_{\alpha}^{\infty} w(x, y)\,\mathrm{d}x\,\mathrm{d}y \tag{1}$$

where $w(x, y)$ is a non-negative weight function describing the distribution of the elementary loops (see [8]).

In order to proceed further it is assumed that the function w can be decomposed, via a separation of variables, into

$$w(\alpha, \beta) = W_{\mathrm{A}}(\alpha)W_{\mathrm{B}}(\beta) \tag{2}$$

for some functions W_{A} and W_{B}. Following [14] these functions can be expressed in terms of f^+ and (1) becomes

$$F(\alpha, \beta) = -\frac{f^+(\beta) + f^+(-\alpha)}{2} + G(\alpha)G(-\beta) \tag{3}$$

where

$$G(\alpha) = \frac{f^+(\alpha) + f^+(-\alpha)}{2\sqrt{f^+(\alpha)}} \qquad \alpha \geqslant 0$$

or

$$G(\alpha) = \sqrt{f^+(-\alpha)} \qquad \alpha < 0.$$

The above equation for $F(\alpha, \beta)$ matches the outer hysteresis loop to within the error of the approximating function $f^+(H)$. The assumption (2) determines the magnetic response inside the major loop and was found in [15] to give good experimental agreement for the magnetic materials tested.

In [8], for F to correspond to a valid Preisach function we observed that it must possess the following properties:

(I) $F(\alpha, \beta) = F(-\beta, -\alpha)$, i.e. symmetry;

(II) $\lim_{\alpha\to\infty} F(\alpha, -\alpha) < \infty$, i.e. hysteresis loop saturates as a finite value;

(III) $\frac{\mathrm{d}F}{\mathrm{d}\beta} \leqslant 0$, $\frac{\mathrm{d}F}{\mathrm{d}\alpha} \geqslant 0$, i.e. magnetic permeability $\frac{\mathrm{d}B}{\mathrm{d}H} \geqslant 0$ everywhere.

Clearly (I) is satisfied automatically. Conditions (II) and (III) will be satisfied if

$$f^+(H) \text{ is strictly increasing} \tag{4}$$

$$\lim_{H\to\infty} f^+(H) = -\lim_{H\to-\infty} f^+(H) \tag{5}$$

and

$$f^+(H) \geqslant -f^+(-H) \qquad \forall H. \tag{6}$$

Each of these three conditions is physically realistic and for accurate measurements any reasonable approximating function should satisfy them. We therefore search for an approximation of the form

$$f^+(H) = \sum_{i=1}^{N} A_i \tanh(P_i H + C_i) \tag{7}$$

where the $\{A_i\}_{i=1}^N$, $\{P_i\}_{i=1}^N$ and $\{C_i\}_{i=1}^N$ are constraints to be determined. Conditions (4) and (5) are automatically satisfied if the constants $\{A_i\}_{i=1}^N$ and $\{P_i\}_{i=1}^N$ are all positive. Similarly, condition (6) will be satisfied if additionally $\{C_i\}_{i=1}^N$ are all non-negative. Thus an approximating function $f^+(H)$ that satisfies (4)–(6) can be found by minimizing the least-squares error subject to the above constraints. This can easily be solved using standard commercial software, for example routine E04KCF of the NAG library [17].

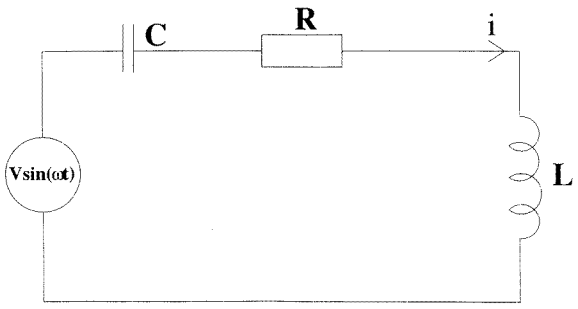

Figure 1. A series LCR circuit.

Table 1. The coefficients used to match the transformer characteristic.

i	A_i	P_i	C_i
1	0.476 31	0.001 1125	0.183 97
2	0.459 64	0.004 4721	0.226 87
3	0.738 76	0.054 8370	2.042 38

3. A ferroresonant LCR circuit

3.1. The circuit equations and numerical integration

The equation for the series LCR circuit (see figure 1) can be written as a set of first-order ordinary differential equations

$$\frac{\mathrm{d}H}{\mathrm{d}t} = \frac{1}{nA}\frac{\sqrt{2}V\sin(\omega t) - V_C - \ell RH/n}{\mu_0 + \frac{\mathrm{d}B}{\mathrm{d}H} + \frac{\ell}{n^2A}L} \tag{8}$$

$$\frac{\mathrm{d}V_C}{\mathrm{d}t} = \frac{H\ell}{Cn} \tag{9}$$

$$\frac{\mathrm{d}B}{\mathrm{d}t} = \frac{\mathrm{d}B}{\mathrm{d}H}\frac{\mathrm{d}H}{\mathrm{d}t} \tag{10}$$

where the independent variables are the applied magnetic field H (A m^{-1}), the magnetic flux density B (teslas) and V_C, the voltage across the capacitor. The parameters are the mean flux path length ℓ (m), the number of turns n on the transformer, the cross sectional area A (m^2), the RMS driving voltage V, the angular frequency $\omega = 2\pi f$, the resistance R (Ω) and the leakage inductance L (A m^{-1}). Note also that the current $i = \ell H/n$.

In order to close the system of equations we need an expression for $\frac{\mathrm{d}B}{\mathrm{d}H}$. This is where the Preisach model and most of the computation comes in. This is calculated by differentiating the last term of (2) or (3) (of [8]) depending on whether H is decreasing or increasing. Thus $\mathrm{d}B/\mathrm{d}H$ ($= \mathrm{d}M/\mathrm{d}H$ plus a constant) is discontinuous whenever $\mathrm{d}H/\mathrm{d}t$ changes sign. It is also discontinuous whenever a maximum or minimum is wiped out since the number of terms in (2) and (3) (of [8]) will change (see the earlier paper [8] for details).

The equations are integrated using a variable-step method suitable for stiff systems. Whenever a discontinuous change in $\mathrm{d}B/\mathrm{d}H$ occurs, the program halts the integration, updates the sets of extrema and then restarts the integration. The initial conditions for the integration are the values of H and V_C at time $t = 0$, the point-of-wave of the forcing cycle and the sets of extrema $\{E_i\}$ and $\{e_i\}$ (i.e. the magnetic history of the material) (again see

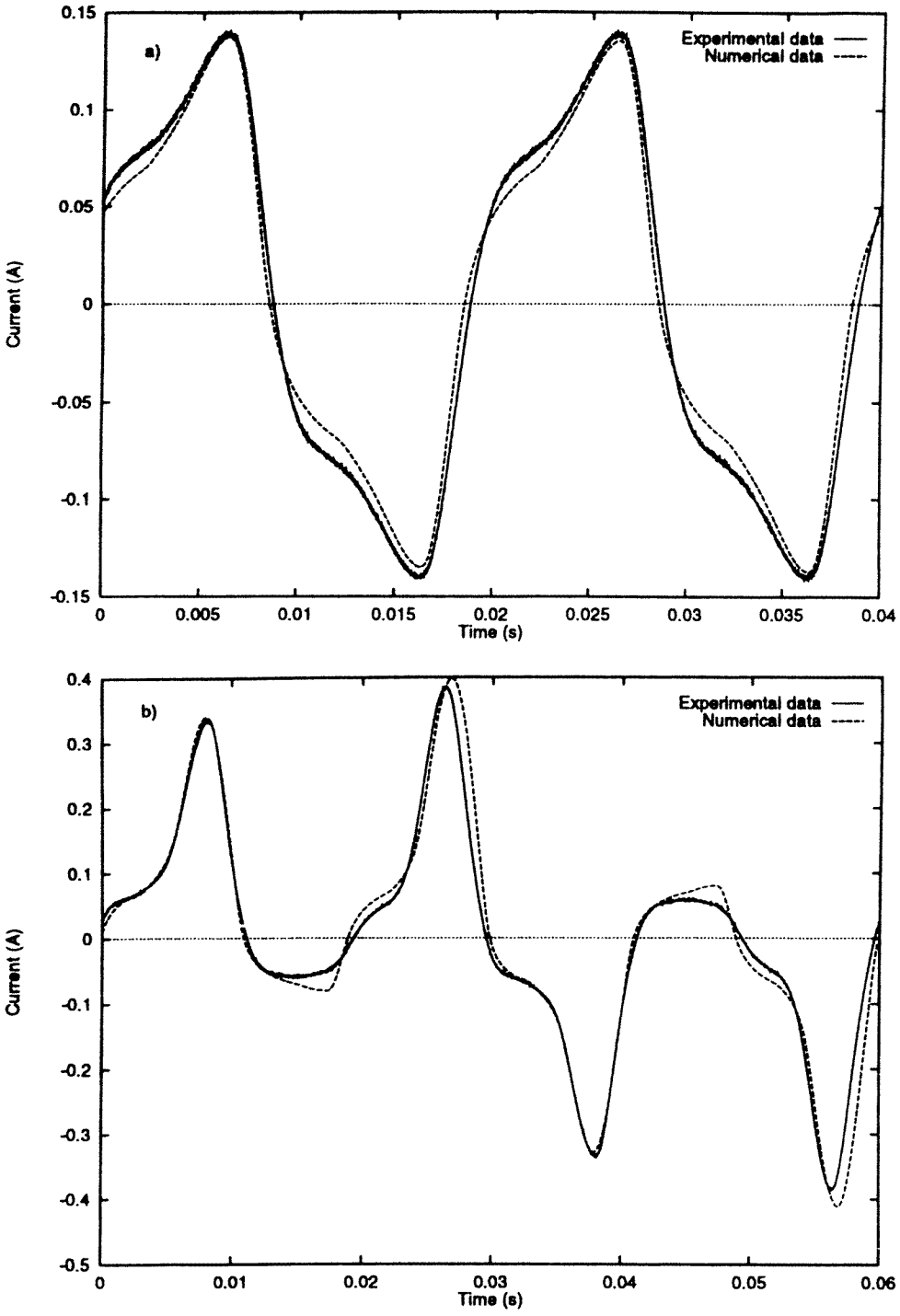

Figure 2. Comparison of current waveforms for (*a*) the non-resonant, (*b*) the period-3 subharmonic resonant and (*c*) the main resonant solutions.

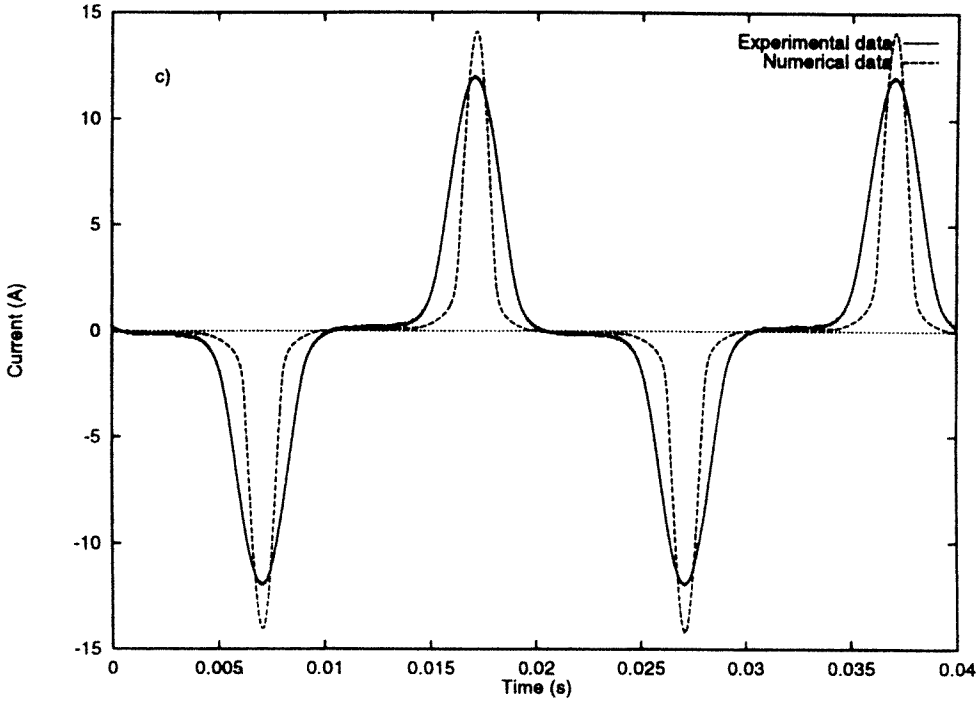

Figure 2. (Continued)

the earlier paper [8] for details). The numerical results are presented in sections 3.2 and 4.

Let us for the moment ignore the term representing the leakage inductance, L, which is usually small (numerically it has been observed that this only affects the amplitude of the main ferroresonance). Then the equations (8)–(10) have seven parameters (for a given B–H characteristic), V, ω, C, R, n, A and ℓ. By making the following coordinate change,

$$V_C' = (n/\ell R)V_C \qquad t' = \omega t$$

we obtain the following system of equations:

$$\frac{\mathrm{d}H}{\mathrm{d}t'} = \frac{R\ell}{\omega n^2 A}\,\frac{\frac{\sqrt{2}Vn}{\ell R}\sin(t') - V_C' - H}{\mu_0 + \frac{\mathrm{d}B}{\mathrm{d}H}} \tag{11}$$

$$\frac{\mathrm{d}V_C'}{\mathrm{d}t'} = \frac{H}{\omega C R} \tag{12}$$

$$\frac{\mathrm{d}B}{\mathrm{d}t'} = \frac{\mathrm{d}B}{\mathrm{d}H}\,\frac{\mathrm{d}H}{\mathrm{d}t'}. \tag{13}$$

Thus we have reduced the number of free parameters to three; note that the B–H characteristic is unchanged. Thus, for any given transformer characteristic, the circuit parameters are given by $\frac{1}{\omega CR}\frac{\sqrt{2}Vn}{\ell R}$ and $\frac{R\ell}{\omega n^2 A}$, and these can be independently varied by changing C, V and A, respectively. In section 4 we shall use each of these parameters as a bifurcation parameter, that is we shall vary each parameter in turn and observe the effect upon the ferroresonant solutions.

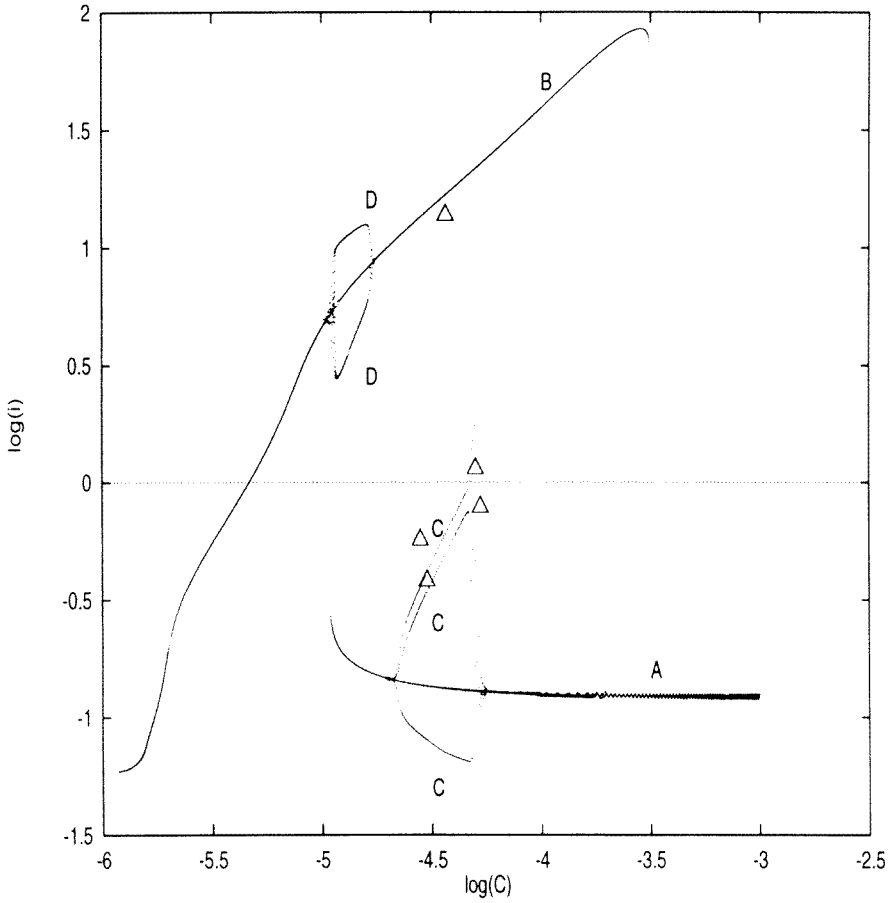

Figure 3. A bifurcation diagram on a log–log scale as the capacitance is varied. The value of the current at each current maximum is plotted against capacitance. See text for a description of the different solutions. △: sample results obtained experimentally.

3.2. Comparison with experiment

Measurements of the flux density B (in teslas) against the applied magnetic field H (in A m^{-1}) were made of the upper bounding curve of a single phase 1 kVA 250 V laboratory transformer. After subtracting off the airline an approximation to the curve of the form (7) with $N = 3$ terms was found using the routine E04KCF from the NAG library [17]. Approximately 30 data points were used covering a large range of positive and negative H with the greatest concentration at the 'knee' of the curve. The routine, which searches iteratively for the optimal coefficients using a modified Newton algorithm, generated different approximations depending upon the random starting conditions used. This is due to the least-squares minimization problem having many local minima but all the approximations generated were suitable with the error being well within the experimental error of the measurements.

The coefficients that were used for the numerical simulations in this paper are given in table 1. These were chosen because they had the smallest residual, approximately 5×10^{-4}. This approximation was incorporated into the Preisach model and the circuit equations, as

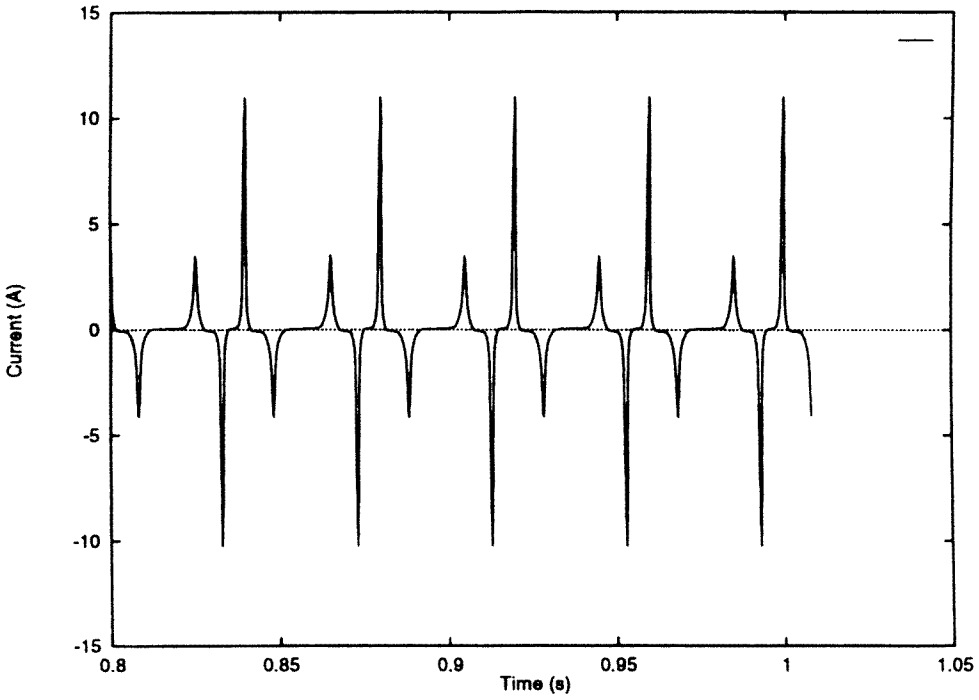

Figure 4. A period-2 solution that bifurcates from the main resonant solution.

described in sections 2 and 3, and [8].

The parameters used to test the numerical simulation were $V = 90$ V, $R = 1.91\ \Omega$, $C = 30\ \mu$F, $f = 50$ Hz, $n = 237$, $A = 0.00252$ m^2, $\ell = 0.434$ m and $L = 0.0017$ A m^{-1}. Thus $\frac{1}{\omega CR} = 55.55$, $\frac{\sqrt{2}Vn}{\ell R} = 36\,390$ and $\frac{R\ell}{\omega n^2 A} = 1.864 \times 10^{-5}$. At these parameters three different stable solutions were observed to occur experimentally: the non-resonant solution, and two ferroresonant solutions—one with a high peak current and the same frequency as the driving voltage (main resonance) and another with a frequency one-third that of the driving voltage and a lower peak current (subharmonic resonance). The numerical and experimental current waveforms for each are compared in figures 2(*a*)–(*c*) respectively and in each case there is excellent agreement. There was also a very close correspondence between the initial conditions and the solution that was reached—an investigation into the dependence upon initial conditions will be reported elsewhere.

4. Bifurcation diagrams

We can now use the numerical simulation to search for other ferroresonant solutions and examine the effect of changing the three independent parameters defined in section 3.

4.1. Varying the capacitance

The same program used to simulate the circuit of section 3.1 was run several thousand times with different values of C and also with random point-of-wave switching, initial charge on the capacitor and magnetic history as defined by $\{E_i\}$ and $\{e_i\}$ (see [8]). All the other parameter values and the B–H characteristic were fixed. Every time that a new

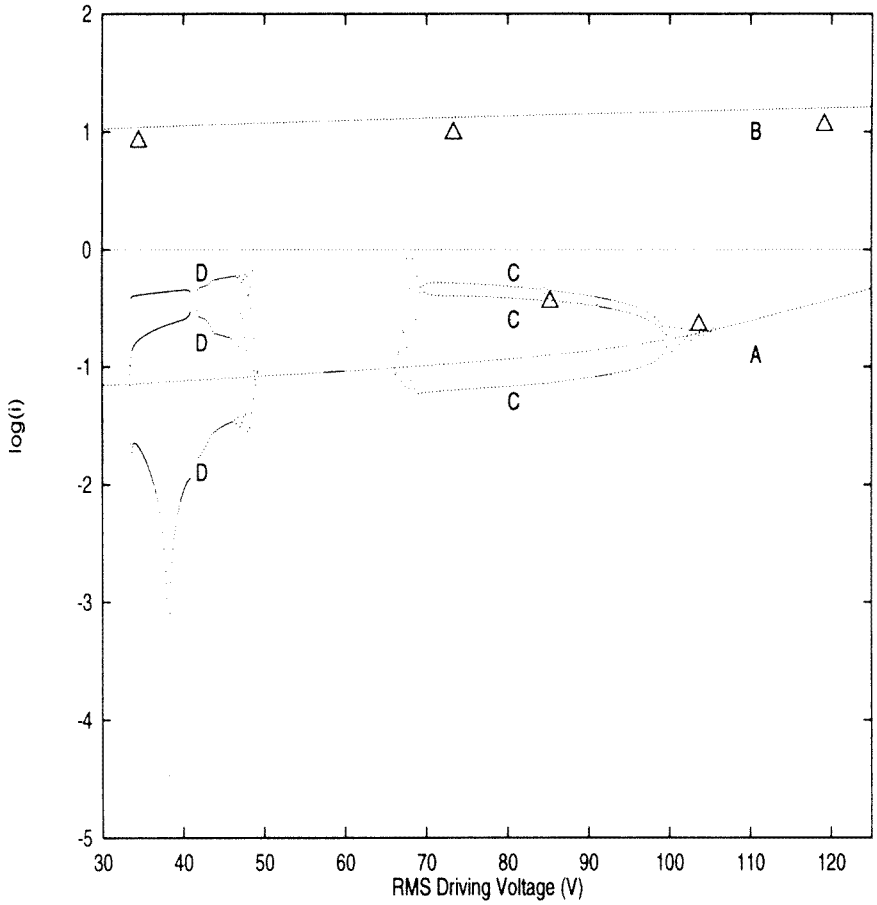

Figure 5. A bifurcation diagram as the RMS driving voltage is varied. The value of the current at each current maximum is plotted against voltage. See text for a description of the different solutions. △: sample results obtained experimentally.

ferroresonant solution was found, the program followed the solution using the capacitance as a bifurcation parameter. In this way a complete bifurcation diagram shown in figure 3 was obtained for the circuit parameters used in section 3.2 for the capacitance range 1–1000 μF.

The vertical axis in figure 3 plots the current value at each current maximum against the capacitance on a log–log scale. Curve A corresponds to the non-resonant solution shown in figure 2(*a*). Because there is just one current maximum per cycle, this is just a single curve. Similarly, curve B is the main resonant solution of figure 2(*c*) and the three curves labelled C are the period-3 subharmonic resonant solutions of figure 2(*b*). Curve D represents a new ferroresonant solution shown in figure 4. This is a period-2 resonant solution that bifurcates from the main resonance and co-exists for a narrow capacitance band. The existence of this new solution was confirmed experimentally at values very close to those predicted by the program. Note, that the curves are composed of several different runs with different initial conditions. This, together with the magnetic memory, gives slightly different values and explains the slight 'fuzziness' of the curves where different runs were spliced together.

If the capacitance is increased beyond 1000 μF there are many other solutions, including

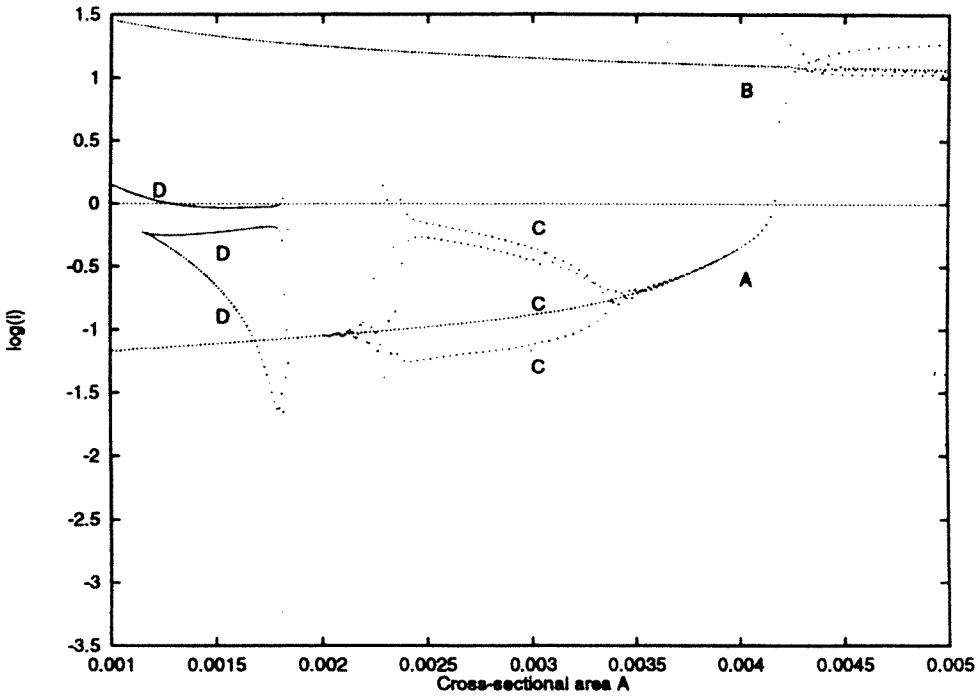

Figure 6. A bifurcation diagram as the cross sectional area, A, of the transformer is varied. The value of the current at each current maximum is plotted against A. See text for a description of the different solutions.

quasiperiodic and chaotic solutions but since they do not co-exist with the non-resonant solution (which has become unstable) we do not consider them here.

4.2. Varying the driving voltage and cross sectional area

We now carry out a similar procedure to the last section, but instead varying the RMS driving voltage between 30 and 150 V (keeping the capacitance fixed at 30 μF); the resulting bifurcation diagram is shown in figure 5.

Again A, B and C represent non-resonant, main resonant and subharmonic (period-3) resonant solutions. Interestingly the period-3 solution loses stability in a period-doubling cascade at around 70 V (see [8]) but regains stability via an inverse cascade at around 50 V. Experiments with the laboratory transformer confirm that the solutions shown lose stability at voltages very close (to within 2 V) to those predicted by figure 5.

Finally, we use the cross sectional area A as a bifurcation parameter, varying between 0.001 and 0.01 m^2. Once more A, B and C represent the three known solutions (figure 6).

As in figure 5 the period-3 solution reappears (labelled D) as the parameter is decreased further. Interestingly, at $A \approx 0.00115$ two of the three current maxima per cycle merge and disappear leaving a period-3 solution with only one current maxima per cycle as shown in figure 7.

In the above we have only varied C, V and A independently. One would need to vary all three together to build up a complete picture of all the existing stable solutions. Nevertheless

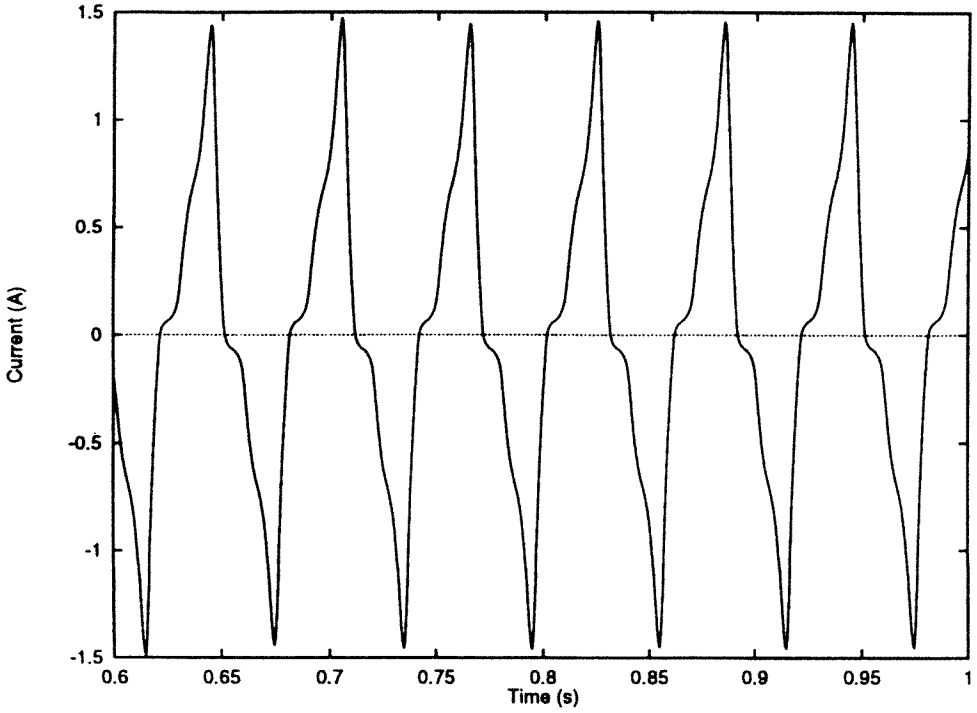

Figure 7. A subharmonic solution with frequency $\frac{1}{3}$ that of the forcing.

we have shown that even a circuit as simple as the one studied has a surprisingly rich and complex behaviour.

5. Conclusions

We have shown that a Preisach representation of a laboratory transformer can be easily calculated from measurements of the major hysteresis loop and excellent agreement with experiment is obtained for a ferroresonant LCR circuit. It should be pointed out that the computational effort needed to compute $f^+(H)$ from the experimental data is negligible. This opens the way for software that can take the raw measurements for the upper bounding curve, together with the circuit configuration and parameters to provide fully nonlinear and hysteretic circuit simulations. To this end, a detailed study of the effect of the quantity and distribution of the data points along the upper bounding curve on the approximation of $f^+(H)$ would be useful.

In addition, we have performed a search for ferroresonant solutions over a wide range of parameters and thus demonstrated the potential predictive power of the numerical simulations. It seems likely that the qualitative features of the bifurcation diagrams and ferroresonant solutions presented here will be similar for transformers with different B–H characteristics and perhaps even for more complicated circuits.

Of course, real power systems are much more complex than the above laboratory system; nevertheless in some circumstances a single-phase ferroresonant system can be reduced to a series LCR circuit. Even where such a reduction is possible, however, the authors have found that a major difficulty is obtaining accurate measurements of the bounding hysteresis curve—

data which the transformer manufacturers often either do not capture or make available. The accurate modelling of the hysteretic properties of transformers is crucial to the prediction of ferroresonant effects and we hope that this work will also stimulate further efforts in the area of data collection.

Acknowledgment

This research was supported by the EPSRC, Research Grant number GR/J69417.

References

[1] Teape J W, Slater R D, Simpson R R S and Wood W S 1976 Hysteresis effects in transformers, including ferroresonance *Proc. Inst. Electr. Eng.* **123** 153–8
[2] Maklad M S and Zaky A A 1976 Multimodal operation of a ferroresonant circuit with quintic nonlinearity *IEEE Trans. Magn.* **12** 380–4
[3] Maklad M S and Fahmy M M 1980 An analytical investigation of a ferroresonant circuit *IEEE Trans. Magn.* **16** 465–8
[4] Marti J R and Soudack A C 1991 Ferroresonance in power systems: fundamental solutions *IEEE Proc.* C **138** 321–9
[5] Araujo A E A, Soudack A C and Marti J R 1993 Ferroresonance in power systems: chaotic behaviour *IEEE Proc.* C **140** 237–40
[6] Mork B S and Stuehm D L 1994 Application of nonlinear dynamics and chaos to ferroresonance in distribution systems *IEEE Trans. Power Deliv.* **9** 1009–17
[7] Chakravarthy S K and Nayar C V 1995 Ferroresonant oscillations in capacitor voltage transformers *IEEE Proc. Circuits Devices Syst.* **142** 30–6
[8] Lamba H, Grinfeld M, McKee S and Simpson R R S 1997 Subharmonic ferroresonance in an LCR circuit with hysteresis *IEEE Trans. Magn.* **33** 2495–500
[9] Germay N, Mastero S and Vroman J 1974 Review of ferroresonance phenomena in a high-voltage power system and presentation of a voltage transformer model for predetermining them *Technical Report* CIGRE3318T
[10] Preisach F 1935 On magnetic after-effect *Z. Phys.* **94** 277
[11] Jiles D C and Atherton D L 1983 Ferromagnetic hysteresis *IEEE Trans. Magn.* **19** 2183–5
[12] Kieny C 1991 Application of the bifurcation theory in studying and understanding the global behaviour of a ferroresonant electric power circuit *IEEE Trans. Power Deliv.* **6** 866–72
[13] Deane J H B 1994 Modelling the dynamics of nonlinear inductor circuits 1994 *IEEE Trans. Magn.* **30** 2795–801
[14] Naidu S R 1990 Simulation of the hysteresis phenomenon using Preisach theory *IEEE Proc.* A **137** 73–9
[15] Hui S Y R and Zhu J 1995 Numerical modelling and simulation of hysteresis effects in magnetic cores using transmission-line modelling and the Preisach theory *IEEE Proc. Electr. Power Appl.* **142** 57–62
[16] Mayergoyz I D 1991 *Mathematical Models of Hysteresis* (New York: Springer)
[17] NAG Mark 16 Documentation